Supplemental Figure Legends

Figure S1. BRCA2 Protects Stalled Replication Forks, But Is Not Involved In Replication Recovery, Related to Figure 1

(A) IdU tract length distributions of DNA fibers in BRCA2-deficient (V-C8) and proficient (V-C8+BRCA2) hamster cells with or without gemcitabine treatment (Gem, 1 μM).

(B) Cumulative distribution curves for IdU DNA fiber tract lengths from mES *BRCA2*$^{lex1/lex2}$ cells and mES cells with and without HU for data shown in Figure 1C (see experimental sketch above graph). The 95% confidence intervals for the cumulative distributions are given in parentheses here and in subsequent figures. Top, graphical sketch of BRCA2 protein in mES *BRCA2*$^{lex1/lex2}$ cells showing deletion of ~200 aa from the C-terminus (the C-ter), including the RAD51 interaction site.

(C) Cumulative distribution curves for IdU tract lengths from CAPAN-1 and CAPAN-1 C2-14 revertant cells with and without HU for data shown in Figure 1D. Top, graphical sketch indicating the BRCA2 protein in CAPAN-1 C2-14 cells. CAPAN-1 has a frame shift mutation leading to a 2002 residue BRCA2 peptide truncated within BRC7 at BRCA2 amino acid 1981. CAPAN-1 C2-14 cells acquired an insertion mutation that restores the reading frame at amino acid 1987.

(D) Examples of DNA fiber images of V-C8 and V-C8+BRCA2 cells upon exposure to HU. Frequency of replication restart and new replication initiation in V-C8 and V-C8+BRCA2 cells with or without HU. *p*-value (two-tailed Student's T-test)

(E) Continuous and non-continuous IdU-CldU tracts in CAPAN-1 and revertant CAPAN-1 C2-14 cells. *p*-values from two-tailed Student's *t*-test.

(F) Sketch outlining interpretation of continuous and gapped tracts given experimental design in CAPAN-1 and revertant CAPAN-1 C2-14 cells (see Figures 1F-H). In the examples shown, lagging strand synthesis continues beyond leading strand synthesis resulting in fork uncoupling.

Figure S2. Characterization of Nascent Strand Shortening by MRE11, Related to Figure 2.

(A-B) Cumulative distribution curves for IdU DNA fiber tract lengths of V-C8 (A) and V-C8+BRCA2 (B) cells during different exposure times to HU for data shown in Figure 2A and 2B, respectively.

(C) Composite length distribution curves for IdU+CldU DNA fiber tract from V-C8 and V-C8+BRCA2 cells with or without HU (left panel) for data shown in Figure 2D and 2E. Median composite tract lengths are given in parentheses. Right panel, cumulative distribution curves with 95% confidence intervals in parentheses.

(D) Cumulative distribution curves for IdU DNA fiber tract lengths of V-C8 and V-C8+BRCA2 cells with or without HU in the presence of MRE11 inhibitor mirin for data shown in Figure 2F.

(E) Cumulative distribution curves for IdU DNA fiber tract lengths of mES *BRCA2*$^{lex1/lex2}$ cells with or without shRNA knockdown of MRE11 in the presence or absence of HU for data shown in Figure 2G.

See also Table S1.

Figure S3. Domain Analysis for BRCA2 Functions During Protection of Stalled Forks, Related to Figure 4.

(A) Western blot of PIR2 stably expressed in V-C8 cells. DR-GFP-reporter assay for HDR events in V-C8 and V-C8+PIR2 cells using flow cytometry after I-SceI expression. (B-C) Cumulative distribution curves for IdU DNA fiber tract lengths of V-C8+PIR2 (B) and V-C8+BRC3-RPA (C) with or without HU for data shown in Figure 4B and 4C, respectively. See also Table S1.

Figure S4. Roles for BRCA2 C-ter and RAD51 during Fork Protection, Related to Figure 5

(A) Blast analysis of deer tick sequence XP_002407637 for conserved domains. E-value for a specific hit: (1) BRCA2DBD (first OB fold of BRCA2) = 2.19e–30; E-value for superfamily hits: (a) BRCA-2_he (4 helix cluster core + 2 beta hairpins) = 2.3e–30, (b) RPA_2b-a (OB fold 1) = 6.3e–38; c : RPA_2-aaRSs_OBF_lik (OB fold 2) = 2.1e–22; d : RPA_2b-a (OB fold 3) = 1.5e–03. The relative position of the putative C-terminal CDK phosphorylation site (red arrow) that we identified in an independent Blast search (Figure 5A) to human BRCA2 is C-terminal of the BRCA2 DNA binding domain.

(B) Cumulative distribution curves for IdU DNA fiber tract lengths of V-C8+BRCA2 S3291A with or without HU for data shown in Figure 5B. See also Table S1.

(C) Western blot for BRCA2 in V-C8, V-C8+BRCA2 and V-C8+BRCA2 S3291A cells.

(D-E) Cumulative distribution curves for IdU DNA fiber tract lengths of mES cells expressing BRC4-flag (D) and *BRCA2*$^{lex1/lex2}$ mES cells expressing mutant RAD51 K133R (E) in the presence or absence of HU for data shown in Figure 5E and 5F, respectively. See also Table S1.

(F) Frequency of replication restart and new replication initiation in mES cells expressing BRC4-flag with or without HU. *p*-values are derived from a two-tailed Student's *t*-test.

Figure S5. Cellular Phenotypes of Mutant and BRCA2 Defective Cells, Related to Figure 6.

(A-B) Chromosomal aberrations from VC-8, VC-8+BRCA2 S3291A and VC-8+BRCA2 cells with or without HU, immediately exposed to colcemid. Plots indicate the % of metaphase spreads with the indicated aberrations (A) and the number of chromosome aberrations per metaphase (B), which are 0.56 and 2.54 for V-C8, 0.25 and 0.8 for V-C8+BRCA2 S3291A, and 0 and 0.2 for V-C8+BRCA2, each with and without HU, respectively). *p*-values are derived from a two-tailed Student's *t*-test. Radial chromosomes include both triradials and quadriradials.

(C) Chromosomal aberrations in V-C8+BRCA2 S3291A cells upon exposure to HU include breaks (black arrowheads, left panel) and radials (enlarged right panels).

(D-E) Survival of indicated V-C8 cell lines upon continuous exposure to 6-thioguanine (6-TG) (D) and mitomycin C (MMC) (E).

Figure S6. Alternative Models, Related To Figure 7.

(A) A replication fork can collapse into a DSB, for example, when the fork encounters a template nick. The separated arm is resected to allow RAD51 filament formation (blue circles) mediated by BRCA2 (pink circle) and strand invasion into the sister to re-establish a replication fork. Such a scenario is unlikely to occur in our experiments as we observe both leading and lagging strand degradation. See also (Budzowska and Kanaar, 2009; Scully et al., 2000).

(B) Alternative fork reversal to Figure 7. If the lagging strand synthesis proceeds farther than leading strand synthesis upon HU, fork reversal yields a 5' ssDNA overhang. Neither BRCA2 nor RAD51 shows a preference for 3' or 5' ssDNA substrates, which are, therefore, equally potent substrates for RAD51 filament formation. In the absence of BRCA2, the filaments are less stable, allowing access of nucleases to the nascent strands, which causes chromosomal instability.

Supplemental Experimental Procedures

DNA Fiber Assay

Cells were plated and allowed to attach before labeling sites of ongoing replication with IdU (50 μM) for 20 or 30 min, followed by exposure to hydroxyurea (4 mM), gemcitabine (1 μM), or untreated media for up to 6 h, as indicated in the figures. Drugs were removed and cells were washed 3 times with phosphate buffered saline (PBS) before labeling with media containing CldU (50 μM) for 20 or 30 minutes to mark sites of replication recovery.

DNA fiber spreads were essentially performed as previously reported (Jackson and Pombo, 1998) with certain modifications. Briefly, cells were harvested and resuspended in cold PBS. The cell suspension was mixed 1:6 with lysis buffer (0.5% SDS, 50 mM EDTA, 200 mM Tris-Cl) and spotted onto a microscope slide (Fisher Scientific), which was carefully tilted in a 15˚ angle to allow spreading of the genomic DNA into single molecule DNA fibers by gravity. Fibers were then fixed in methanol and acetic acid (3:1) and subsequently acid treated with HCl (2.5 N) to denature the DNA fibers. Slides were neutralized and washed with PBS (1x pH 8.0, 3x pH 7.4) before blocking with 10% goat serum and 0.1% Triton-X in PBS for at least 1 h. Slides were incubated with primary antibodies against IdU (BD Biosciences, anti-BrdU clone B44, 1:100 in blocking buffer) and CldU (Novus Biologicals, anti-BrdU BU1/75(ICR1), 1:200 in blocking buffer) and secondary antibodies (Invitrogen, Alexa Fluor 488 goat anti-mouse, 1:200 in blocking buffer and Alexa Fluor 555 goat anti-rat, 1:300 in blocking buffer) for 1 h each. Slides were

mounted in Prolong with DAPI (Invitrogen) prior to analysis using an Olympus BX60 microscope.

Fibers were analyzed using ImageJ software. See Table S1 for the numbers of fibers and independent experiments performed for each condition. The median replication tract length and *p*-values derived from the Mann-Whitney test were calculated using Prism software. In addition, 95% confidence intervals were calculated for each cumulative distribution, which were tested for normality using the D'Agostino-Pearson test (Table S1). The rate for nascent replication tract degradation was estimated using the published conversion of 2.59 kb/μm (Jackson and Pombo, 1998).

BAC Engineering

The human bacterial artificial chromosome (BAC) clone RP11-777I19, which contains the full *BRCA2* genomic region (Sharan et al., 2004), was obtained from BACPAC Resource Center at the Children's Hospital Oakland Research Institute in Oakland, California. Using the Cre-loxP recombination system, a floxed *neo* (kanamycin) gene, that is expressed both from a prokaryotic and eukaryotic promoter (PL452, (Liu et al., 2003)), was inserted into the RP11-777I19 vector backbone using EL350 bacteria (Lee et al., 2001). Briefly, 100 ng of a 1.8 kb BamHI/EcoRI fragment containing the floxed kanamycin/G418 resistance cassette was electroporated into EL350 containing RP11-777I19 (1.75 kV, 25 μF and 200 ohms) which had been induced to express Cre recombinase by prior growth in media with 0.1% L(+)arabinose for 1 h. After electroporation, bacteria recovered 1

h at 30°C and were then grown on LB plates containing 12.5 µg/ml chloramphenicol and 12.5 µg/ml kanamycin. Site-specific insertion of the kanamycin/G418 resistance cassette into loxP of RP11-777I19 was verified by PCR using forward primer NCA-35, 5'-TGGTGAATTGACTAGTGGGTAGATC-3', which primes in the vector backbone 5' of the loxP site, and reverse primer NCB-38, 5'-GCCTACCGGTGGATGTGGAATG-3', which primes in the kanamycin/G418 resistance cassette, (600 bp PCR fragment, 30 cycles of 94°C for 45 sec, 58°C for 45 sec and 72°C for 1 min). Furthermore, the integrity of the genomic insert in RP11-777I19neo was verified by comparing the restriction patterns of NotI, EcoRI and NotI/NheI digests with that of the parental RP11-777I19 BAC. Nucleotide exchanges that result into a serine (TCT) to an alanine (GCG) codon change at amino acid position 3291 in exon 27 of BRCA2 were introduced into RP11-777I19neo using recombineering technology as described in (Warming et al., 2005). Oligos RecA3, 5'-TTGAGTAGACTGCCTTTACCTCCACCTGTTAGTCCCATTTGTACATTTGTTGCGCCTGTTGACAATTAATCATCGGCA-3' and RecB3, 5'-GTATTTGGTGCCACAACTCCTTGGTGGCTGAAATGCCTTCTGTGCAGCCGGTCAGCACTGTCCTGCTCCTT-3'were used to amplify the *galK* cassette. Oligos RecA4, 5'-GAGTAGACTGCCTTTACCTCCACCTGTTAGTCCCATTTGTACATTTGTTGCGCCGGCTGCACAGAAGGCATTTCAGCCACCAAGGAGTTGTGGCACCAAA-3' and RecB4, 5'-TTTGGTGCCACAACTCCTTGGTGGCTGAAATGCCTTCTGTGCAGCCGGCGCAACAAATGTACAAATGGGACTAACAGGTGGAGGTAAAGGCAGTCTACTC-3' were annealed to generate a double-stranded DNA oligo that was used to replace the *galK* cassette. In order to validate the nucleotide exchanges in RP11-777I19neo3291a, PCR was

performed using primers NCA38, 5'-ATGTCTTCTCCTAATTGTGAG-3' and NCB40, 5'-CTCACATTCTTCCGTACTGGC-3' (567 bp PCR fragment, 33 cycles of 94°C for 45 sec, 58°C for 45 sec and 72°C for 45 sec). The codon change results in an additional HhaI restriction site, which was verified by restriction digest. In addition, the 567 bp PCR fragment was sequenced. Furthermore, the integrity of the genomic insert in RP11-777I19neo3291a was verified by comparing the restriction patterns of SpeI or NheI digests with that of the parental RP11-777I19neo BAC.

Generation of BAC-complemented VC-8 cells

12 μg of RP11-777I19neo or RP11-777I19neo3291a was linearized with PI-SceI and stably transfected into V-C8 cells containing DR-GFP (Saeki et al., 2006) using GenePORTER Transfection Reagent (Genlantis). Clones with randomly integrated RP11-777I19neo were selected with 300 μg/ml G418 and genomic DNA analyzed by PCR using primers NCA-35 and NCB-38, as described above. Clones with randomly integrated RP11-777I19neo3291a were selected with 1 mg/ml G418. Expression of BRCA2 protein in V-C8+BRCA2 and V-C8+BRCA2 S3291A cells was confirmed by Western blot analysis. V-C8+BRCA2 clone #3 was used to study I-SceI-induced DSB repair and to study sensitivity to MMC and HU. V-C8+BRCA2 S3291A clone #22 was used to study I-SceI-induced DSB repair.

BRCA2 Western Blot

Sub-confluent V-C8+BRCA2 or V-C8+BRCA2 S3291A cells that were grown for 24 h were harvested and lysed in ice-cold NETN-450 buffer [450 mM NaCl, 1 mM EDTA,

20 mM Tris (pH 8.0), and 0.5% Igepal CA-630] for 15 min on ice. Cell debris was removed by centrifugation and an equal amount of NETN-0 [1 mM EDTA, 20 mM Tris (pH 8.0), and 0.5% Igepal CA-630] was added and centrifuged again. Supernatant containing 100 µg protein of total protein was boiled in SDS blue loading buffer (New England Biolabs), separated on a NuPAGE Novex Mini gel (Tris-acetate 3-8%) and transferred onto a nitrocellulose membrane. BRCA2 protein was detected by probing the blot with polyclonal antibody anti-BRCA2 (Ab-2) (1:50, Calbiochem) for 1 h at room temperature, followed by two washes with Tris-bufferd saline + Tween-20 (TBS-T) for 15 min each, and another incubation with HRP-conjungated rabbit IgG (1:10000, Novus Biologicals) for 1 h at room temperature. After one 15 min and two 5 min washes with TBS-T, signals were detected with the ECL detection system (GE Healthcare). As a loading control, levels of α-tubulin were determined by stripping off antibodies with Restore Western Blot Stripping Buffer (Pierce), and subsequently re-probing with monoclonal anti-α-Tubulin clone DM 1A (1:5000, Sigma) followed by HRP-conjungated ECL anti-mouse IgG (1:10000, Amersham).

I-SceI-induced double-strand break repair

$5x10^6$ V-C8+PIR2 cells were transfected with 50µg of an I-SceI expressing vector pCBASce by electroporation (280 V, 1000 µF) as reported in ref (Pierce and Jasin, 2005; Saeki et al., 2006). 48 hours later, GFP-positive cells were counted using Becton Dickinson FACScan and analyzed with CellQuest software (Becton Dickinson).

Supplemental References

Budzowska, M., and Kanaar, R. (2009). Mechanisms of Dealing with DNA Damage-Induced Replication Problems. Cell Biochemistry and Biophysics *53*, 17-31.

Jackson, D.A., and Pombo, A. (1998). Replicon Clusters are Stable Units of Chromosome Structure: Evidence That Nuclear Organization Contributes to the Efficient Activation and Propagation of S Phase in Human Cells. The Journal of Cell Biology *140*, 1285-1295.

Lee, E.C., Yu, D., Martinez de Velasco, J., Tessarollo, L., Swing, D.A., Court, D.L., Jenkins, N.A., and Copeland, N.G. (2001). A highly efficient Escherichia coli-based chromosome engineering system adapted for recombinogenic targeting and subcloning of BAC DNA. Genomics *73*, 56-65.

Liu, P., Jenkins, N.A., and Copeland, N.G. (2003). A highly efficient recombineering-based method for generating conditional knockout mutations. Genome Res *13*, 476-484.

Pierce, A.J., and Jasin, M. (2005). Measuring recombination proficiency in mouse embryonic stem cells. Methods Mol Biol *291*, 373-384.

Saeki, H., Siaud, N., Christ, N., Wiegant, W.W., van Buul, P.P., Han, M., Zdzienicka, M.Z., Stark, J.M., and Jasin, M. (2006). Suppression of the DNA repair defects of BRCA2-deficient cells with heterologous protein fusions. Proc Natl Acad Sci U S A *103*, 8768-8773.

Scully, R., Puget, N., and Vlasakova, K. (2000). DNA polymerase stalling, sister chromatid recombination and the BRCA genes. Oncogene *19*, 6176-6183.

Sharan, S.K., Pyle, A., Coppola, V., Babus, J., Swaminathan, S., Benedict, J., Swing, D., Martin, B.K., Tessarollo, L., Evans, J.P.*, et al.* (2004). BRCA2 deficiency in mice leads to meiotic impairment and infertility. Development *131*, 131-142.

Warming, S., Costantino, N., Court, D.L., Jenkins, N.A., and Copeland, N.G. (2005). Simple and highly efficient BAC recombineering using galK selection. Nucleic Acids Res *33*, e36.

Figure S1.

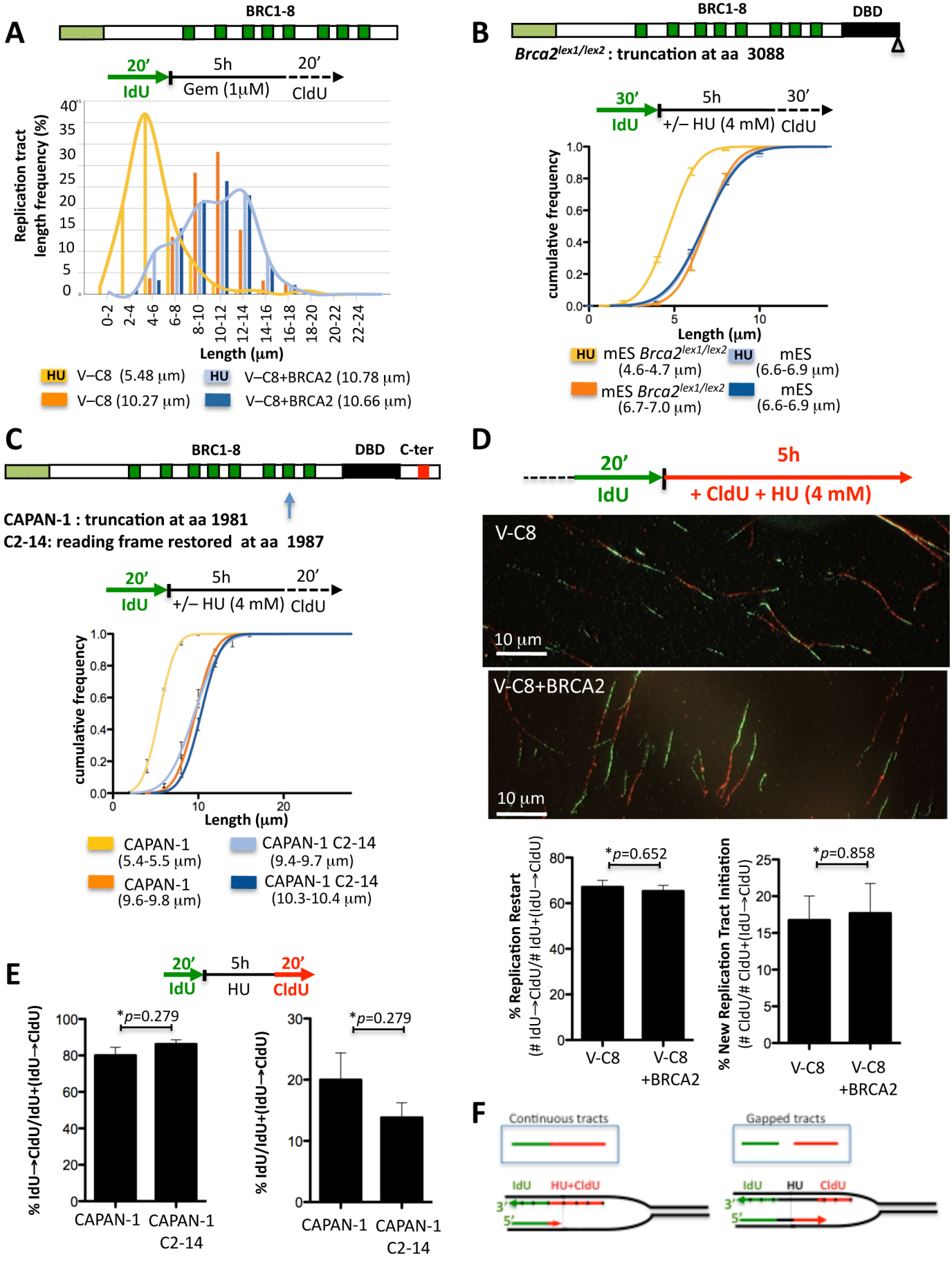
A
BRC1-8
20′ IdU
5h Gem (1μM)
20′ CldU
Replication tract length frequency (%)
Length (μm)
HU V–C8 (5.48 μm)
V–C8 (10.27 μm)
HU V–C8+BRCA2 (10.78 μm)
V–C8+BRCA2 (10.66 μm)
B
BRC1-8
DBD
Brca2lex1/lex2 : truncation at aa 3088
30′ IdU
5h +/– HU (4 mM)
30′ CldU
cumulative frequency
Length (μm)
HU mES Brca2lex1/lex2 (4.6-4.7 μm)
HU mES (6.6-6.9 μm)
mES Brca2lex1/lex2 (6.7-7.0 μm)
mES (6.6-6.9 μm)
C
BRC1-8
DBD
C-ter
CAPAN-1 : truncation at aa 1981
C2-14: reading frame restored at aa 1987
20′ IdU
5h +/– HU (4 mM)
20′ CldU
cumulative frequency
Length (μm)
CAPAN-1 (5.4-5.5 μm)
CAPAN-1 C2-14 (9.4-9.7 μm)
CAPAN-1 (9.6-9.8 μm)
CAPAN-1 C2-14 (10.3-10.4 μm)
D
20′ IdU
5h + CldU + HU (4 mM)
V-C8
10 μm
V-C8+BRCA2
10 μm
% Replication Restart (# IdU→CldU/# IdU+(IdU→CldU))
*p=0.652
V-C8
V-C8 +BRCA2
% New Replication Tract Initiation (# CldU/# CldU+(IdU→CldU))
*p=0.858
V-C8
V-C8 +BRCA2
E
20′ IdU
5h HU
20′ CldU
% IdU→CldU/IdU+(IdU→CldU)
*p=0.279
CAPAN-1
CAPAN-1 C2-14
% IdU/IdU+(IdU→CldU)
*p=0.279
CAPAN-1
CAPAN-1 C2-14
F
Continuous tracts
Gapped tracts
IdU
HU+CldU
IdU
HU
CldU
3′
5′

Figure S2.

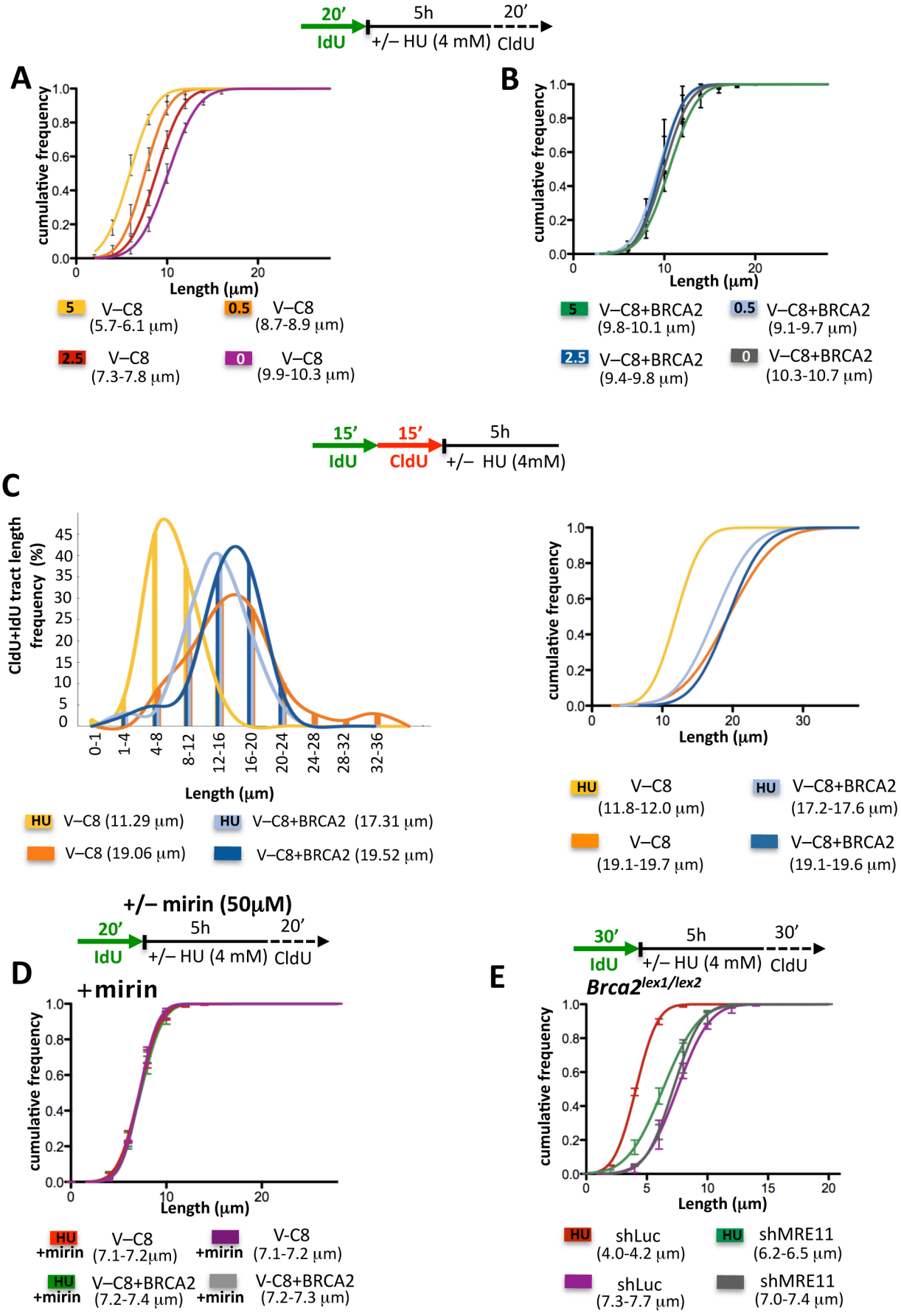
20′
IdU
5h
+/– HU (4 mM)
20′
CldU
A
cumulative frequency
Length (μm)
5 V–C8 (5.7-6.1 μm)
0.5 V–C8 (8.7-8.9 μm)
2.5 V–C8 (7.3-7.8 μm)
0 V–C8 (9.9-10.3 μm)
B
cumulative frequency
Length (μm)
5 V–C8+BRCA2 (9.8-10.1 μm)
0.5 V–C8+BRCA2 (9.1-9.7 μm)
2.5 V–C8+BRCA2 (9.4-9.8 μm)
0 V–C8+BRCA2 (10.3-10.7 μm)
15′
IdU
15′
CldU
5h
+/– HU (4mM)
C
CldU+IdU tract length frequency (%)
0-1
1-4
4-8
8-12
12-16
16-20
20-24
24-28
28-32
32-36
Length (μm)
HU V–C8 (11.29 μm)
HU V–C8+BRCA2 (17.31 μm)
V–C8 (19.06 μm)
V–C8+BRCA2 (19.52 μm)
cumulative frequency
Length (μm)
HU V–C8 (11.8-12.0 μm)
HU V–C8+BRCA2 (17.2-17.6 μm)
V–C8 (19.1-19.7 μm)
V–C8+BRCA2 (19.1-19.6 μm)
+/– mirin (50μM)
20′
IdU
5h
+/– HU (4 mM)
20′
CldU
D
+mirin
cumulative frequency
Length (μm)
HU +mirin V–C8 (7.1-7.2μm)
+mirin V-C8 (7.1-7.2 μm)
HU +mirin V–C8+BRCA2 (7.2-7.4 μm)
+mirin V-C8+BRCA2 (7.2-7.3 μm)
30′
IdU
5h
+/– HU (4 mM)
30′
CldU
E
Brca2lex1/lex2
cumulative frequency
Length (μm)
HU shLuc (4.0-4.2 μm)
HU shMRE11 (6.2-6.5 μm)
shLuc (7.3-7.7 μm)
shMRE11 (7.0-7.4 μm)

Supplemental Figure 3

Figure S3.

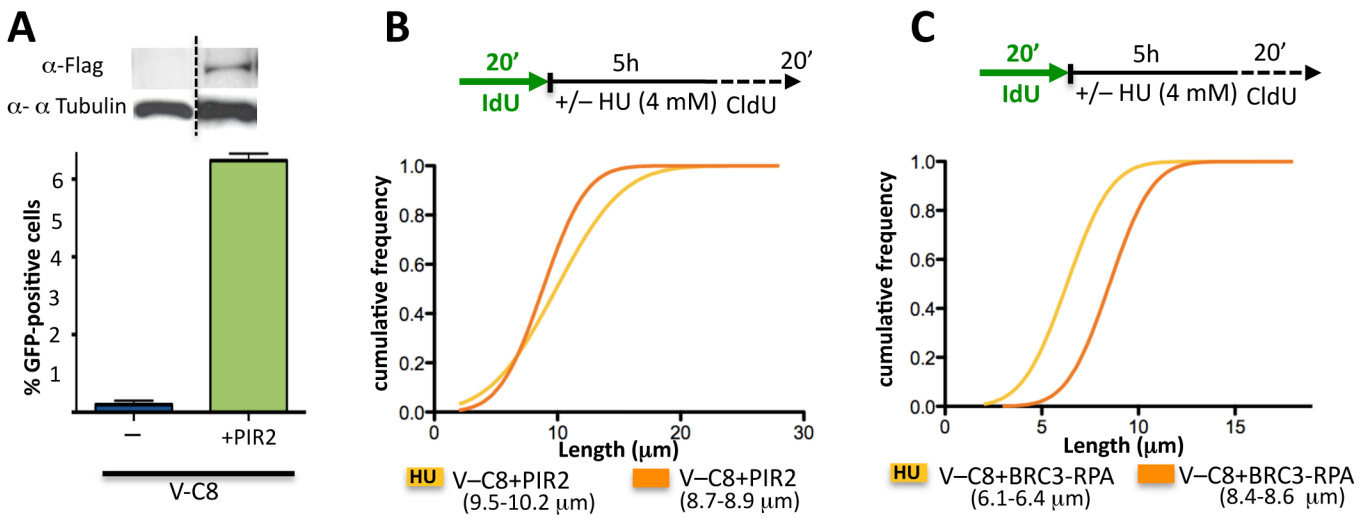

Figure S4.

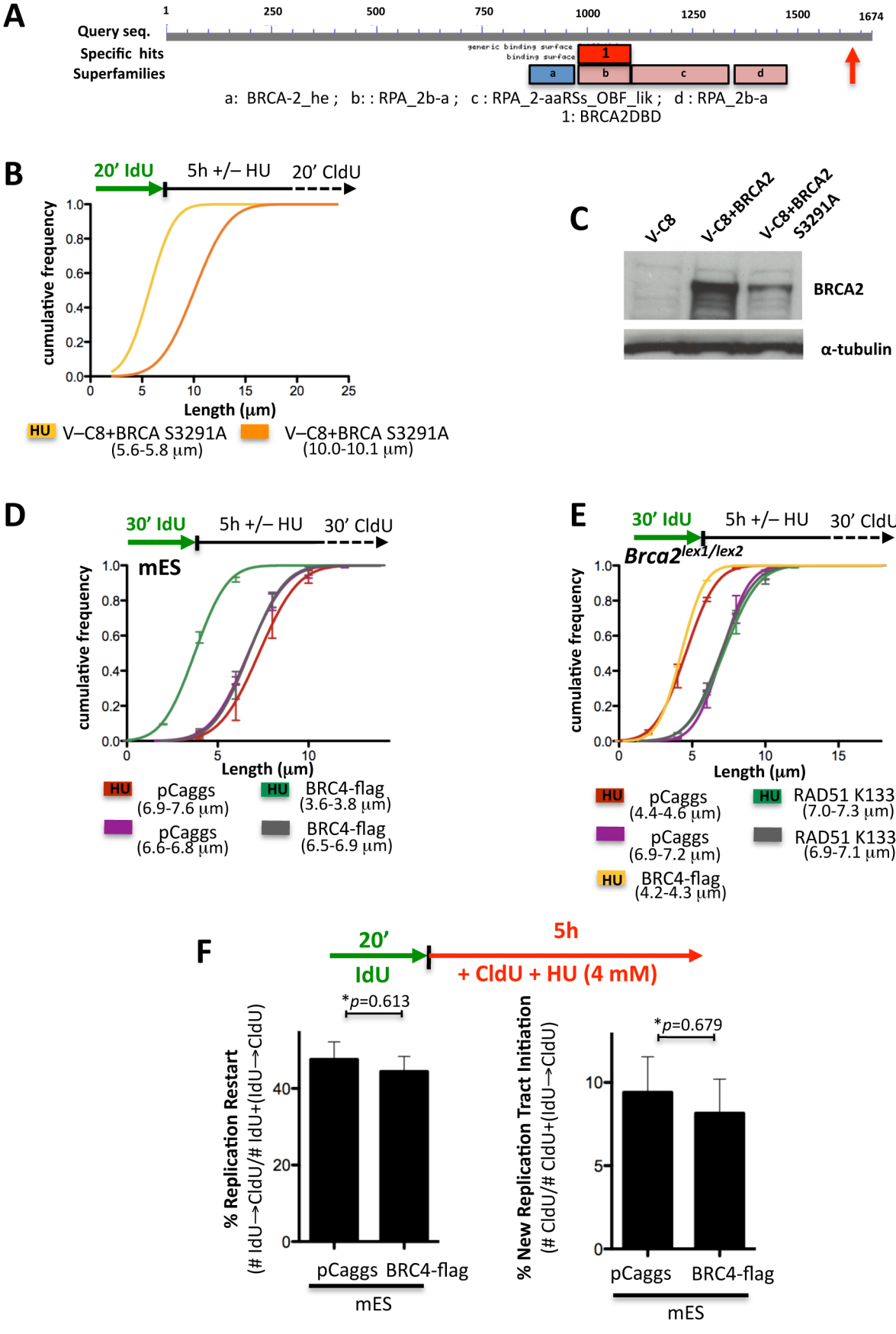
A
1
250
500
750
1000
1250
1500
1674
Query seq.
Specific hits
Superfamilies
generic binding surface
binding surface
1
a
b
c
d
a: BRCA-2_he ; b: : RPA_2b-a ; c : RPA_2-aaRSs_OBF_lik ; d : RPA_2b-a
1: BRCA2DBD
B
20' IdU
5h +/– HU
20' CldU
cumulative frequency
Length (μm)
HU V–C8+BRCA S3291A (5.6-5.8 μm)
V–C8+BRCA S3291A (10.0-10.1 μm)
C
V-C8
V-C8+BRCA2
V-C8+BRCA2 S3291A
BRCA2
α-tubulin
D
30' IdU
5h +/– HU
30' CldU
mES
cumulative frequency
Length (μm)
HU pCaggs (6.9-7.6 μm)
pCaggs (6.6-6.8 μm)
HU BRC4-flag (3.6-3.8 μm)
BRC4-flag (6.5-6.9 μm)
E
30' IdU
5h +/– HU
30' CldU
Brca2lex1/lex2
cumulative frequency
Length (μm)
HU pCaggs (4.4-4.6 μm)
pCaggs (6.9-7.2 μm)
HU BRC4-flag (4.2-4.3 μm)
HU RAD51 K133R (7.0-7.3 μm)
RAD51 K133R (6.9-7.1 μm)
F
20' IdU
5h + CldU + HU (4 mM)
*p=0.613
% Replication Restart
(# IdU→CldU/# IdU+(IdU→CldU)
pCaggs
BRC4-flag
mES
*p=0.679
% New Replication Tract Initiation
(# CldU/# CldU+(IdU→CldU)
pCaggs
BRC4-flag
mES

Supplemental Figure 5

Figure S5.

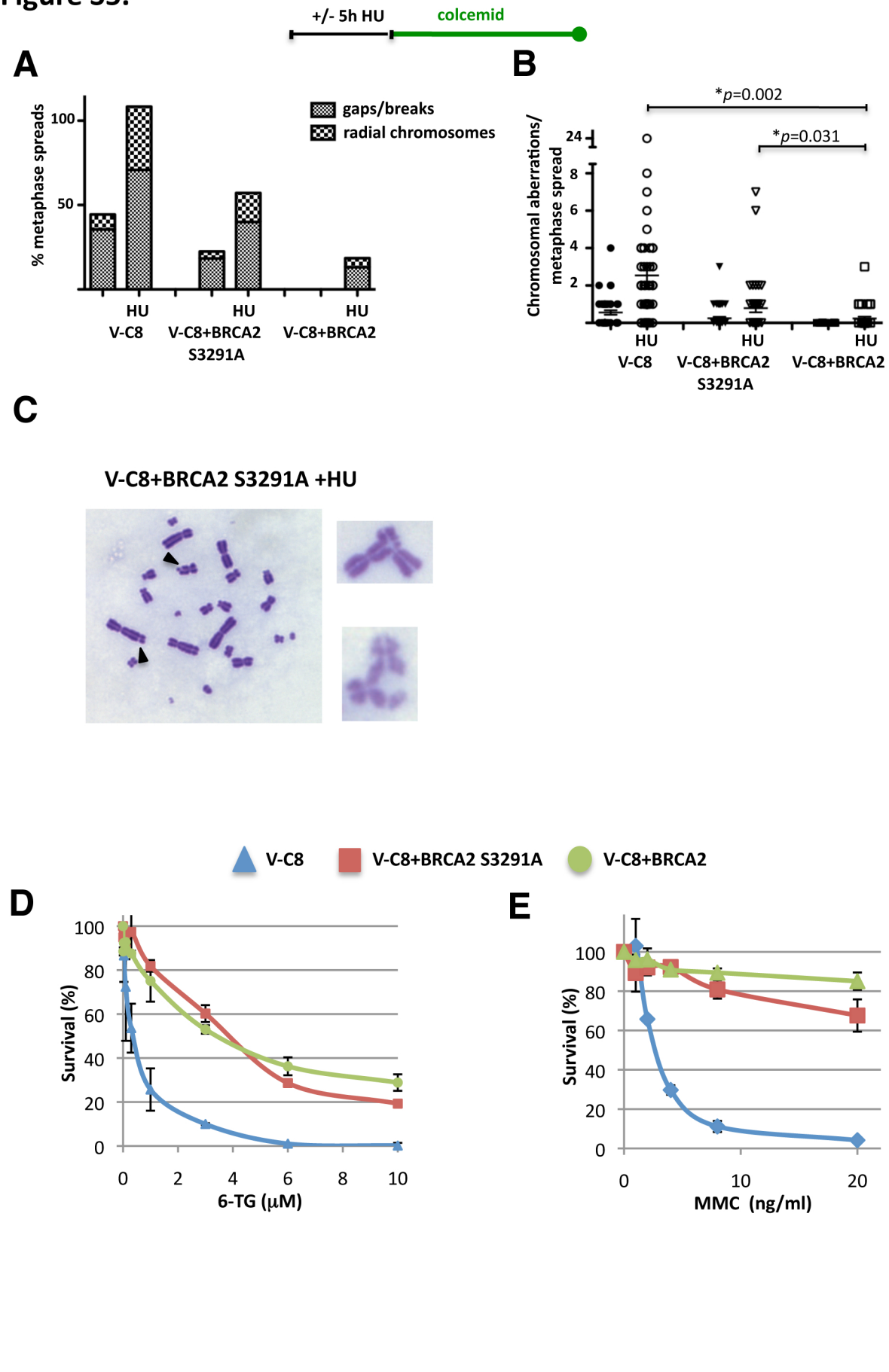

Supplemental Figure 6

Figure S6.